The Nucleus, **46** (1-2) 2009: 37-42

The Nucleus
A Quarterly Scientific Journal of Pakistan
Atomic Energy Commission
NCLEAM, ISSN 0029-5698

SYNTHESIS AND CHARACTERIZATION OF $Zn_{1-x-y}Cd_xLi_yO_\delta$ SOLID SOLUTION

M. KAMRUZZAMAN[1], M. K. R. KHAN[2], M. M. RAHMAN[2], *M. A. S. KARAL[1]

M. SHAHJAHAN[2] and M. G. M. CHOWDHURY[2]

[1]Department of Physics, Bangladesh University of Engineering and Technology, Dhaka-1000, Bangladesh

[2]Department of Physics, University of Rajshahi, Rajshahi-6205, Bangladesh

(Received November 26, 2008 and accepted in revised form February 24, 2009)

$Zn_{1-x-y}Cd_xLi_yO_\delta$ (x=0.30; y=0.05, 0.10, 0.15, 0.20 and δ= 0.975, 0.95, 0.925, 0.90) samples have been prepared by conventional solid state reaction method and studied their electrical, magnetic and structural properties. The dc electrical resistivity measurement shows that all samples are highly resistive (~10^6 ohm-cm) upto a transition temperature (T_t), above which resistivity falls drastically that reveals the samples are semiconducting in nature and T_t decreases with increase of Li. The activation energies vary from (0.74-0.51) eV depending on doping concentrations, i.e. the activation energy is lower for higher concentration of Li in the solution. Magnetic mass susceptibility measurement shows negative sign that indicate the samples are diamagnetic. From XRD analysis, there exist two phases one is hexagonal ZnO and another is cubic CdO which suggests the formation of superlattice structure of the system. Crystallite size at planes (100), (002), (101), (102), (110), (103), (200), (112) and (111), (200), (220) for ZnO and CdO ranges from 20 to 50 nm and for Li ranges from 27 to 40 nm.

Keywords: Zinc oxide, Lithium, Solid solution, DC resistivity, Mass susceptibility, XRD

1. Introduction

Zinc oxide (ZnO) is one of the most promising materials due to its unique combination of attractive properties like non-toxicity, good electrical, optical such as light emitting diode (LED), laser diode (LD) in ultra-violet or blue spectral and piezoelectric behavior with its low cost [1-4]. The excellent optical properties of ZnO make it suitable for use in surface acoustic wave devices [5], electrodes in solar cells [6], flat panel displays [7] and for energy conversion and storage [8]. To achieve applicable ZnO based opto-electronic devices, there have been considerable experimental investigations focused on the preparation of p-type ZnO sample and its band gap engineering by impurity doping and various alloying methods [9-10].

On the other hand, cadmium oxide (CdO) is important due to its applications, specifically in the field of optoelectronic devices such as solar cells [11-12], photo transistors [13] and diodes [14], transparent electrodes [15], gas sensors [16], etc. These applications of CdO are based on its specific optical and electrical properties. For example, CdO films show a high transparency in the visible region of the solar spectrum, as well as a high ohmic conductivity. The intensity of optical and electrical effects of CdO depends on the deviations from the ideal CdO stoichiometric, as well as on the size and shape of the particles [17].

ZnO is a hexagonal wurtzite-type structure and an exitonic binding energy of ~60meV much larger than ~25 meV of CdO, which permits the efficient exitonic stimulated ultra-violet emission even at room temperature [18-19]. So, both ZnO and CdO have high transparency in the visible and near infrared region and both show n-type conductivity.

CdO has direct band gap of 2.2-2.7 eV [20] and indirect band gap of 1.36 eV [21]. So CdO presents the advantage of a low resistivity with respect to the high values obtained for ZnO, but this exhibits a higher transparency, having a room temperature band gap ~3.2 eV [22]. Obviously, it is

* Corresponding author : asayem221@yahoo.com

difficult to obtain a high transmission coefficient in the visible region and conductivity qualities simultaneously [23]. However, a ternary compound which combines these properties in a controlled way may allow the optimization of the window layer.

A various means of oxide alloying with ZnO in thin film form investigated but to our knowledge there are no such reports in bulk form. Considering immense application of ZnO and CdO, our aim is to prepare highly conducting Cd and Li (x=0.30 and y=0.05, 0.10, 0.15, 0.20) doped ZnO by solid state reaction method and studied their electrical, magnetic and structural properties.

The electrical property was observed by measuring the change of resistivity with temperature and the magnetic property measurement was carried out by the magnetic mass susceptibility balance (The Mark 1 MSB). Structure and crystallite size were determined from XRD analysis.

2. Experimentals

2.1. Sample preparation

$Zn_{1-x-y}Cd_xLi_yO_\delta$ (x=0.30; y=0.05, 0.10, 0.15, 0.20 and δ= 0.975, 0.95, 0.925, 0.90) samples were synthesized by solid-state reaction method. Stoichiometric appropriate amounts of the chemicals of high purity reagent grade ZnO, $CdCO_3$ and Li_2CO_3 were weighted out separately and kept in an allumina crucible. These chemicals were ground for 1.5 hours and thoroughly mixed. The gray powder thus obtained was scrapped from the wall of the mortar and placed in an allumina crucible. The crucible alongwith the powder was placed in the furnace (digital muffle furnace) and heated from room temperature to 600 ºC for 12 hours. Then the furnace was switched off and allowed to cool to room temperature. When cooled down to room temperature, the sample was taken out and ground until it becomes fine powder. This procedure was repeated for second time at 700 ºC, called second calcination and again ground into fine powder. The powder was then put in a dice (sample holder) and pressed into pellets of about 13 mm diameter and 2-3 mm thick under a pressure of 90 KN/m^2 for about 5 minutes using a hand pressure machine. The prepared pellets were then placed in a ceramic boat. The boat with pellet was inserted into the furnace for sintering in air atmosphere at 900 ºC for 12 hours and furnace cooled to obtain crystalline phase. For both calcination and sintering the heating and the cooling rate were 10ºC/min and 5ºC/min respectively.

2.2. Conductivity measurement

The resistances of samples were measured by two-probe method. The resistivity, ρ of the samples was calculated using formula [24].

$$\rho = \frac{RA}{L} \quad (1)$$

where, R is the resistance, A is the area and L is the thickness of the sample.

The two ends of the junctions on the surface were connected to a digital voltmeter and an ammeter. The two junctions were also connected in series to a stabilized dc current source, used for measuring the current in the input circuit. One end of the copper constantan thermocouple was placed on the base of the sample while the other ends were placed in another digital voltmeter for measuring millivolts. The temperatures corresponding to the e.m.f. generated by the thermocouple were extracted from calibration chart. The sample was heated slowly with the help of an ac current using a variac ~1μA current was applied to the circuit. At each heating state the current, the potential drop and the thermo e.m.f. were collected simultaneously.

2.3. Mass susceptibility measurement

The magnetic mass susceptibility balance (The Mark 1 MSB) work on the basis of stationary sample and moving magnets as shown in Fig.1. Two pairs of magnets are placed at opposite ends of a beam making a balanced system having a magnetic field at each end. Introduction of the sample into the magnetic field attempts to deflect the beam and the movement is optically detected.

A compensating force was applied by introducing a current through a coil between the other pair of magnets. The current required to maintain the original position of the balance beam is proportional to the force created by the sample; and the direction that the beam (magnetic field) moves indicate whether the sample is paramagnetic or diamagnetic which is shown by a plus or minus indication on the display.

The magnetic mass susceptibility χ_g in c.g.s. units was calculated using relation [25].

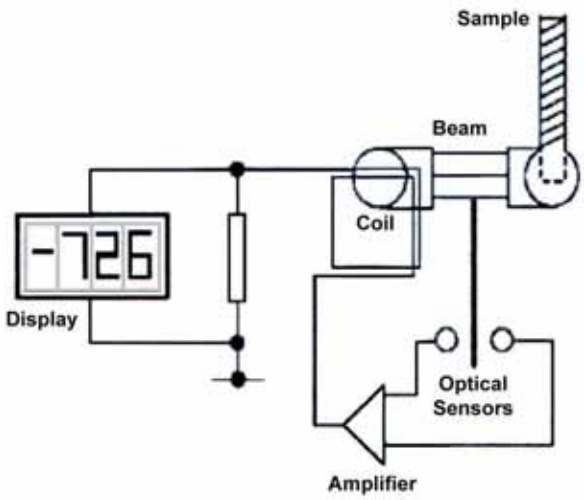

Figure 1. Magnetic mass susceptibility balance.

$$\chi_g = \frac{C \times L \times (R - R_0)}{10^9 m} \qquad (2)$$

where,

C= Calibration constant of the balance (=2.086)

R= Reading of sample in tube

R_0= Reading of empty tube (normally –ve)

L= Length of sample in cm. (L>1.5 cm)

m= Mass of sample in grams

For diamagnetic material χ_g is negative and for paramagnetic material χ_g is positive.

2.4. XRD analysis

The crystalline phase of the materials were checked by X-ray diffractometer using CuK_α radiation (λ=1.5405 Å, or 0.154 nm) at room temperature. The diffraction scan was recorded in the angular range 10º ≤ 2θ ≤ 80º with a scanning speed of 2º/min, and step sampling of 0.02º. The crystallite size was determined qualitatively using Scherrer method [26].

$$\xi = \frac{k\lambda}{B\cos\theta} \qquad (3)$$

where, λ is the wavelength of the incident X-ray beam k is a constant equal to unity and θ is Bragg angle. In general, B is full width at half-maximum (FWHM) of a diffraction peak expressed in radians.

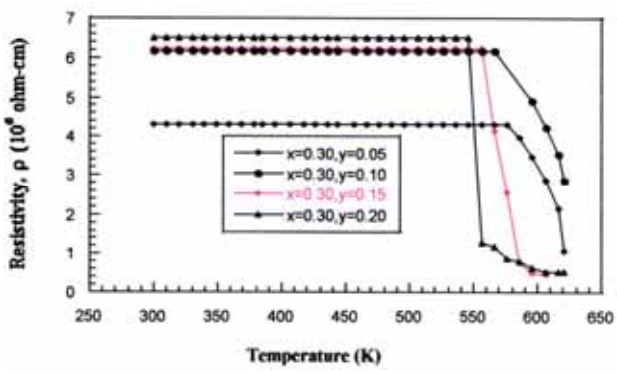

Figure 2. Temperature dependence of electrical resistivity for $Zn_{1-x-y}Cd_xLi_yO_\delta$.

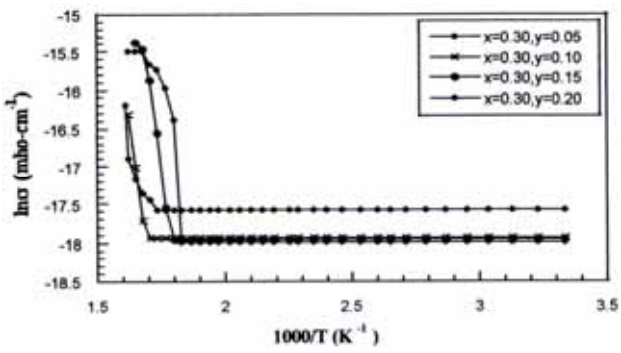

Figure 3. Inverse temperature dependence of conductivity for $Zn_{1-x-y}Cd_xLi_yO_\delta$

3. Results and Discussion

Temperature dependence of electrical resistivity in Fig. 2 shows the samples are semiconducting in nature and the magnitude of the resistivity is strongly dependent on the doping concentrations. The resistivity of the samples increases with the increase of Li which can reduce the carrier concentration because of its small ionic radius [27] and the resistivity remains constant upto a certain transition temperature (T_t≥550 K), after which resistivity falls very sharply. It is established that the conductivity of ZnO influenced by the presence of excess Zn atoms or introduction of impurity atoms. Since the amount of Cd is constant, it seems the conductivity of doped ZnO is mostly due to excess Zn rather than Li and

Cd doping. However, the doping concentrations affect the transition temperature T_t significantly. After T_t the conductivity increases sharply due to more electrons transition occurs from valance band to conduction band. The value of the transition temperature (T_t) is lower for higher Li and vice-versa as shown in Fig. 4. The Conductivity decreases with increase of Li suggesting that the degree of disorder is increased. The same result also explained for ZnO:Li [28] which revealed an increase of the extent of the localized states near the mobility edge with increasing the disorder in the structure. It is worthy to mention that Li ratio has pronounced effect on the transition temperature with Li [29-30].

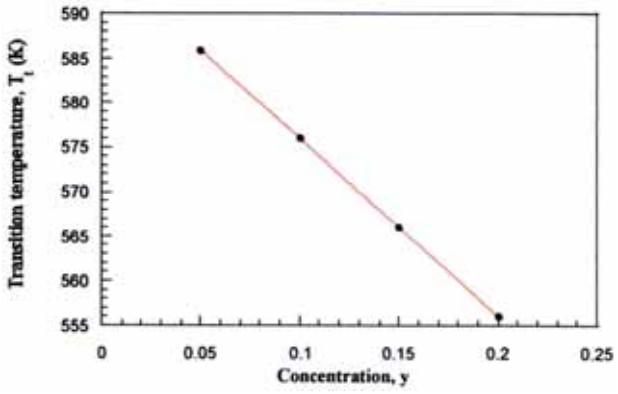

Figure 4. Transition temperature of $Zn_{1-x-y}Cd_xLi_yO_{\delta}$.

Activation energy, ΔE was calculated from Fig. 2 at temperature 596K using formula [31].

$$\Delta E = -\frac{\ln \sigma}{1/T} K_B \qquad (4)$$

where, σ is the conductivity, T is the temperature and K_B is the Boltzmann constant.

Table 1. Activation energy for $Zn_{1-x-y}Cd_xLi_yO_{\delta}$

x and y (x=0.30)	Transition temp T_t (K)	Conductivity σ (mho-cm^{-1})	Activation energy ΔE(eV)
y= 0.05	587	2.312x10^{-8}	0.74
y= 0.10	576	1.625x10^{-8}	0.66
y = 0.15	566	1.609 x 10^{-8}	0.61
y= 0.20	556	1.542x10^{-8}	0.51

The activation energies for different samples are tabulated in Table 1 that shows the activation energy is lower for higher Li. The decrease of conductivity with Li was attributed to the combined effect of the decrease of both the ionic and the electronic conductivity. The decrease of electronic conductivity was also contributed by both the decrease of concentration of hopping carriers and the accompanied decrease of the electron mobility [32].

The magnetic mass susceptibility measurement shows that the samples have negative mass susceptibility and obtained values are tabulated in Table 2. Reported values of mass susceptibility for ZnO = -46.0x10^{-6} c.g.s units and CdO = -30.0x10^{-6} c.g.s units. The obtained values in this study are close to the reported values [33].

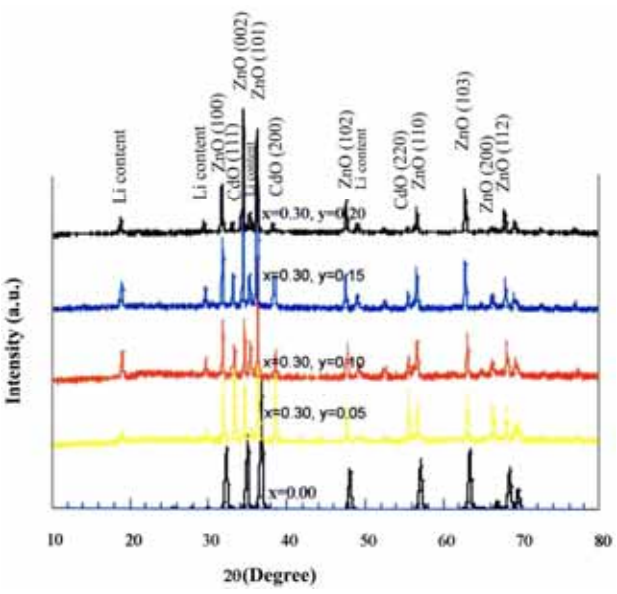

Figure 5. XRD pattern for $Zn_{1-x-y}Cd_xLi_yO_{\delta}$.

The XRD patterns for $Zn_{1-x-y}Cd_xLi_yO_{\delta}$ are shown in Fig. 5 which reveals that all samples are very good crystalline in nature and preferently oriented. For pure ZnO, diffraction peaks identified as (1 0 0), (0 0 2), (1 0 1), (1 0 2), (1 1 0), (1 0 3), (2 0 0) and (1 1 2) planes. There are three distinct peaks at angles (2θ values) 33.26°, 38.58° and 55.54°, correspond to planes (1 1 1), (2 0 0) and (2 2 0) are appeared in addition to the ZnO peaks. Analyzing the peak positions of the spectrogram with standard JCPDS (Joint Committee on Powder Diffraction Standards) cards (Grant in Aid report

Table 2. Magnetic mass susceptibility for $Zn_{1-x-y}Cd_xLi_yO_\delta$

x and y (x=0.30)	Mass of the empty tube (gm)	Mass of the sample tube (gm)	Mass of the sample m (gm)	Reading of the empty tube (R_0)	Reading of the sample tube (R)	Length of the sample L (cm)	Calibration constant of Balance (C)	Magnetic mass susceptibility x 10^{-6}
y=0.05	1.5741	1.7086	0.1345	-62	-76	2.3	2.086	-49.9
y=0.10	1.5131	1.6899	0.1768	-30	-48	3.0	2.086	-63.7
y=0.15	1.5311	1.5311	0.1389	-54	-74	2.3	2.086	-69.0
y=0.20	1.7778	1.998	0.2190	-16	-32	3.1	2.086	-47.2

Table 3. Crystallite size of ZnO at different (hkl) planes for $Zn_{1-x-y}Cd_xLi_yO_\delta$

x and y (x=0.30)	Crystallite size (nm) for different (hkl) planes							
	(1 0 0)	(0 0 2)	(1 0 1)	(1 0 2)	(1 1 0)	(1 0 3)	(2 0 0)	(1 1 2)
y=0.05	44	46	42	35	33	32	25	26
y=0.10	42	49	44	46	33	30	-	33
y=0.15	38	44	38	35	33	-	25	26
y=0.20	40	44	40	29	26	21	42	28

1987) both for ZnO and CdO, it is clear that the spectrogram is the combination of two crystal structures-one for hexagonal ZnO and other for cubic CdO. Considering these two structures, the lattice parameters were found consistent with reported values both for the hexagonal ZnO and cubic CdO structure. There are also four extra peaks found at around 20°, 30°, 35° and 50° for Li content phase. Crystallite size for ZnO and CdO in different crystallographic planes is tabulated in Tables 3 and 4. The values obtained are consistent with the estimated values [34].

Table. 4. Crystallite size of CdO at different (hkl) planes for $Zn_{1-x-y}Cd_xLi_yO_\delta$

x and y (x=0.30)	Crystallite size (nm) for different (hkl) planes		
	(1 1 1)	(2 0 0)	(2 2 0)
y=0.05	44	35	34
y=0.10	42	38	38
y=0.15	42	40	33
y=0.20	42	42	32

4. Conclusions

From resistivity measurement the samples are semiconducting in nature and the resistivity increases with increase of Li. After transition temperature T_t, conductivity increases sharply because thermally assisted direct transition of electrons from valence band to conduction band. The negative mass susceptibility suggests that the material is diamagnetic. From XRD analysis there exist hexagonal ZnO and cubic CdO phase in the $Zn_{1-x-y}Cd_xLi_yO_\delta$ system which indicates the formation of superlattice structure of the system.

Acknowledgements

The authors would like to express their thanks to Professor Dr. Makoto Ishida, Department of Electrical and Electronic Engineering, Toyohashi University of Technology, Japan and Dr. M. Shahjahan, a researcher under supervision of Makoto Ishida for assistance in X-ray diffraction experiment.

References

[1] Z.C. Jin, J. Hamberg and C. G. Granqvist, J. Appl. Phys. **64** (1988) 5117.

[2] J. B. Yoo, A. L. Fahrenbruch and R. H. Bube, J. Appl. Phys. **68** (1990) 4694.

[3] D. M. Bagnall, Y. F. Chen, Z. Zhu, T. Tao, S. Koyama, M. Y. Shen and T. Goto, Appl. Phys. Lett. **70** (1997) 2230.

[4] Z. K. Tang, G. K. L. Wong, P. Yu, M. Kawasaki, A. Ohtomo, H. Koinuma and Y. Segawa, Appl. Phys. Lett. **72** (1998) 3270.

[5] C. K. Lau, S. K. Tiku and K.M. Lakin, J. Electrochem. Soc. **127** (1980) 1843.

[6] G. Cordillo, Surf. Rev. Lett. **9** (2002) 1675.

[7] H.L. Hartnagnel, A. L. Dawar, A. K. Jain and C. Jagadish, Semiconducting transparent thin films, Institute of Physics Publishing , USA, Philadelphia, PA (1995)

[8] Y.C. Kong, D.P. Yu, W. Fang, B. Zhang and S. Q. Feng, Appl. Phys. Lett. **87** (2001) 407.

[9] M. Kawasaki, A. Ottoman, I. Ohkubo, H. Koinuma, Z.K. Tang, P. Yu, G. K. L. Wong, B. P. Zhang and Y. Segawa, Mater. Sci. Eng. **B 56** (1998) 249.

[10] Y. Yanta, S.B. Zhang and S. T. Pantelides, Phys. Rev. Lett. **86** (2001) 5723.

[11] C. Sravani, K.T.R. Reddy, O. M. Hussain, and P. J. Reddy, J. Solar Energy. Soc. India, **1** (1996) 6.

[12] L. M. Su, N. Grote and F. Schmitt, Electron. Lett. **20** (1984) 716.

[13] R. Kondo, H. Okimura and Y. Sakai, Jpn. J. Appl. Phys. **10** (1971) 1547.

[14] F. A. Benko and F. P. Koffyberg, Solid State Commun. **57** (1986) 901.

[15] A. Shiori, Jpn. Patent No. 7 (1997) 909.

[16] D. R. Lide (Ed.), CRC Handbook of Chemistry and Physics, 77th edn., CRC Press, Boca Raton, 1996/1997, 3/278, p. 12/97.

[17] M. Risti´c, S. Popovi´c and S. Musi´c, Mater. Lett. **58** (2004) 2494.

[18] P. Zu, Z. K. Tang, G. K. L. Wong, M. Kawasaki, A. Ohtomo, H. Koinuma and Y. Segawa, Solid State Commun. **103** (1997) 459.

[19] J. Narayan, K. Dovidenko, A. K. Sharma and S. Oktyabrsky, J. Appl. Phys. **84** (1998) 2597.

[20] K. L. Chopra and S. Ranyan Das, Thin Film Solar Cells, Plenum Press, New York (1993)

[21] K. Gurumurugan, D. Mangalaraj and S. K. Narayandass, J. Cryst. Growth **147** (1995) 355.

[22] C. Sravani, K. T. R. Reddy and P. J. Reddy, Mater. Lett. **15** (1993) 356.

[23] K. L.Chopra, S. Major and D.K. Pandya, Thin Solid Films **102, (**1983) 1.

[24] D. Halliday, R. Resnick and J. Walker, Fundamentals of Physics (Sixth Edition), John Wiley & Sons, Inc. (2001) p. 619.

[25] Magnetic Susceptibility Balances Model Mark 1 MSB.htm.

[26] B.D. Cullity, Elements of X-ray diffraction, Addison-Wesley Publishing Co. Inc. (1967) p.102.

[27] P. Wu, J. Zhong, N.W. Emanetoglu, Y. Chen, S. Muthukumar, and Y. Lu, J. Electronic Matters, **33(6)** (2004) 1.

[28] J. Tauc, R. Grigorovici and A. Vancu, Phys. Stat. Sol. **15** (1966) 627.

[29] A. Onodera, N. Tamaki, Y. Kawamura, T. Sawada and H. Tamashita, Jpn. J. Appl. Phys. **35** (1996) 5160.

[30] A. Onodera, N. Tamaki, Y. Kawamura, T. Sawada, N. Sakagami, K. Jin, H. Satoh and K. H. Yamashita, J. Kor. Phys. **32** (1998) S11.

[31] N. F. Mott and E. A. Davis, Electronic Processes in Non-Crystalline Materials, Clarendon Press, Oxford (1979)

[32] Ch. H. Lee and G. M. Choi, Solid State Ionics **135** (2000) 653.

[33] Magnetic Properties Susceptibilities Chart from READE.htm.**1/1/97.**

[34] M. K. R. Khan, M. M. Rahman and I. Tanaka, The Nucleus **39**, Nos. 3-4 (2002) 149.